RESEARCH ON TORQUE DYNAMIC COORDINATED CONTROL OF A NOVEL DUAL POWER SOURCE THRESHING DRUM OF COMBINE HARVESTER

/

新型双动力源脱粒滚筒扭矩动态协调控制研究

Zhihao ZHU[1)], Xiaoyu CHAI *[1)], Lizhang XU[2)], Li QUAN[3)], Chaochun YUAN[4)], En LU[1)], Shuofeng WENG[3)], Shichao TIAN[1)], Guangqiao CAO[5)]

[1)]School of Agriculture Engineering, Jiangsu University, 212013, China
[2)]Key Laboratory for Theory and Technology of Intelligent Agriculture Machinery and Equipment, Jiangsu University, 212013, China
[3)]School of Electrical and Information, Jiangsu University, 212013, China
[4)]Automotive Engineering Research Institute, Jiangsu University, 212013, China
[5)]Nanjing Institute of Agricultural Mechanization, Ministry of Agriculture and Rural Affairs, 211200, China
Tel: 18852832940; E-mail: xfpaxy521123@163.com
DOI: https://doi.org/10.35633/inmateh-76-41

***Keywords**: Combine harvester, threshing drum, electric drive, torque compensation*

ABSTRACT

In response to the issues faced by conventional combine harvesters' threshing drums, such as the difficulty in maintaining stable speed due to load fluctuations and torque disturbances, as well as the limited speed adjustment range to adapt to changes in crop varieties and properties, this study proposes a novel dual power source threshing drum (DPSTD). By incorporating a power coupling device and a motor into the existing mechanical structure, the DPSTD utilizes the flexible speed and torque output capabilities of the motor to achieve a wide speed adjustment range and enhance its resistance to interference. A robust model predictive control strategy is designed based on finite time disturbance observer (FTDO) to compensate for torque under load fluctuations. Simulation results demonstrate that the DPSTD can achieve rapid and accurate speed regulation. Moreover, under torque disturbances and load mutations, the DPSTD with the torque compensation control strategy, can reduce the speed error by 73.90%. This significantly improves the speed tracking performance of the threshing drum, exhibiting good anti-interference capabilities. Finally, the superiority of the DPSTD is validated through bench tests, confirming its effectiveness and feasibility and providing new insights for control research on threshing drums.

摘要

针对传统联合收获机脱粒滚筒面对负载波动和扭矩干扰时难以稳速影响作业效果，以及调速范围小难以适应作物品种和属性的变化等问题，本文基于并联式混合动力技术提出了一种新型双动力源脱粒滚筒 (DPSTD)，通过在原有的机械驱动结构上加入动力耦合装置和电机，利用电机灵活的转速和转矩输出功能实现脱粒滚筒的大范围调速并提高抗干扰能力。本文对 DPSTD 各部件进行数学建模，并设计了基于有限时间干扰观测器 (FTDO) 的电机鲁棒模型预测控制策略，以实现 DPSTD 在负载波动和干扰下的扭矩补偿，进一步对 DPSTD 的调速和稳速性能进行研究，仿真结果表明，DPSTD 可以快速精准地进行转速调节，并且在存在扭矩干扰和负载突变的情况下，采用扭矩补偿的控制策略的 DPSTD 可以将脱粒滚筒的转速误差均方根值降低 73.90%，最大转速误差降低 76.18%，冲击度均方根值降低 33.51%，最大冲击度降低 73.18%。可明显改善模式切换平顺性和脱粒滚筒转速跟踪效果，具备较好的抗干扰能力。最后台架试验进一步验证了 DPSTD 的调速和稳速性能，证明了其有效性和可行性，为联合收获机脱粒滚筒控制研究提供了新思路。

INTRODUCTION

The combine harvester is one of the widely used core agricultural machinery in agricultural production *(Sun et al., 2018)*. With the development of agricultural automation technology, there is an increasing demand for automatic control of combine harvesters *(Chen et al., 2017; Shojaei, 2021)*. The threshing drum has always been considered a core component of the combine harvester and has been extensively studied *(Vlădut et al., 2022; Zhang et al., 2024; Hou et al., 2023; Li et al., 2023)*.

Zhihao Zhu, Student; Xiaoyu Chai, Lecture; Lizhang Xu, Research fellow; Li Quan, Professor; Chaochun Yuan, Professor; En Lu, Associate professor; Shuofeng Weng, Student; Shichao Tian, Student; Guangqiao Cao, Research fellow

Resistance to interference and speed control are important research directions in the control of threshing drums, and they are of significant importance for enhancing the overall functionality and operational performance of the machine *(Olaye et al., 2016; Sudajan et al., 2002; Alizadeh and Khodabakhshipour 2010). Zhang et al (2011)* designed a robust control method for the threshing drum speed in a combine harvester, with the travel speed and feeding rate of the harvester as control variables and the drum speed as the controlled variable. The effectiveness of this method was verified through simulations and experiments. *Qin et al (2009)* proposed a mathematical model for the walking, harvesting, and threshing system of a combine harvester, which can effectively simulate the actual working process of the harvester. *Zhang et al (2023)* designed a control system based on active disturbance rejection and dynamic matrix modeling. This approach achieved real-time control of the drum speed and compensation of the control delay.

However, due to the limitations of the mechanical structure in conventional combine harvesters, the control of the threshing drum speed is typically achieved indirectly through the vehicle speed and feeding rate. This approach suffers from drawbacks such as low speed control accuracy, time delays, reduced operational efficiency, and the inability to adjust the speed according to changes in crop varieties and properties. In recent years, the research and application of electrification technology in agricultural machinery are becoming increasingly widespread *(Khatawkar et al., 2019; Scolaro et al., 2021; Mocera, & Somà, 2022; Zhu et al., 2023)*. Electric motors offer advantages such as fast response, high driving efficiency, and a wide range of speed and torque outputs. These advantages can effectively enhance the flexibility and efficiency of agricultural equipment. *Yang et al (2022)* conducted an electrification transformation of the reaping and threshing components of a combine harvester and designed a control system for the motors. Furthermore, they tested the system's speed tracking and anti-clogging functionalities in wheat harvesting experiments, and the results indicated that the system exhibited favorable practicality. *Sahoo & Raheman (2020)* developed a pure electric small rice harvester driven by two DC motors. Field test results showed that the product has high operational efficiency and endurance, and can effectively reduce environmental pollution and harvesting costs. *Wang et al (2020)* electrified the reaping part of a combine harvester, conducted finite element simulation on its mechanical structure, and designed a control method for the motor. Field test results showed that the modified harvester can automatically adjust its reaping speed according to the travelling speed, thereby improving the operational performance.

The purpose of this article is to improve the anti-interference capability of the threshing drum and broaden its speed range to adapt to the harvesting requirements of various crops using electric drive technology. However, considering that the threshing drum is the most power-demanding component in a combine harvester, relying solely on electric motor drive would require the installation of high-power motors and a high-power supply system, resulting in higher costs. Therefore, this article retains the original mechanical transmission components and proposes a novel dual power source threshing drum that combines an electric motor with a power coupling device. The power coupling device diverts power from both the motor and the engine, allowing the threshing drum to achieve a wide speed range. By incorporating an additional smaller electric motor. Additionally, the torque compensation provided by the electric motor enhances the threshing drum's anti-interference capability, enabling stable and high-quality operation.

In this study, a dual power source threshing drum (DPSTD) is proposed and an electric motor robust model predictive control system based on disturbance observer is designed. Furthermore, the speed control and torque compensation functions of the DPSTD are validated through simulation and bench test.

MATERIALS AND METHODS

Architecture of the DPSTD

The specific structure of the newly designed DPSTD for a combine harvester, as depicted in Fig.1, incorporates a power coupling device with a planetary gear set to distribute the power from both the engine and the motor. The power coupling device comprises a reducer, a sun gear, an outer planetary carrier, and an inner planetary carrier. The central shaft of the primary gear of the reducer serves as Input 1 of the power coupling device (connected to the motor), while the secondary gear of the reducer is coaxially integrated with the sun gear. The inner planetary carrier has an outer gear ring and an inner gear ring, the outer gear ring meshes with the outer planetary carrier, the inner gear ring meshes with the sun gear, the central axis is the input 2 of the power coupling device (connected to the engine source power output shaft), and the central axis of the outer planetary carrier is the output end of the power coupling device (connected to the threshing drum). The motor power is transmitted through the reduction set, resulting in torque amplification, and then delivered to the sun gear. Simultaneously, the engine power is transmitted to the inner planetary carrier.

As the inner planetary carrier engages with both the sun gear and the outer planetary carrier, the engine power and the motor power are combined and transmitted through the outer planetary carrier to drive the threshing drum. The speed of the engine source power output shaft remains relatively stable during operation. By adjusting the motor speed, the speed regulation function of the threshing drum is achieved to adapt to different harvesting conditions.

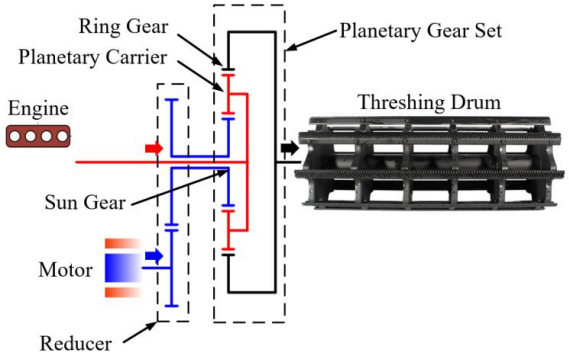

Fig. 1 - Structure of the DPSTD

The DPSTD has three power modes: hybrid mode, conventional mode, charging mode, and reversal mode, as shown in Fig. 2. In the hybrid mode, the threshing drum is driven by the engine and the motor. This mode is used when the engine's allocated power to the threshing drum during the harvesting process is lower than the instantaneous power required for threshing or when the preset mechanical speed of the threshing drum does not match the actual required speed. In the conventional mode, the threshing drum is solely driven by the engine. This mode is used when the power provided by the engine to the threshing drum meets the operational load requirements, and the preset speed of the threshing drum satisfies the harvesting needs of the current crop. In reversal mode, the threshing drum is driven by the motor to rotate in the opposite direction. This mode is used for special working conditions where the drum is overloaded and causes blockage.

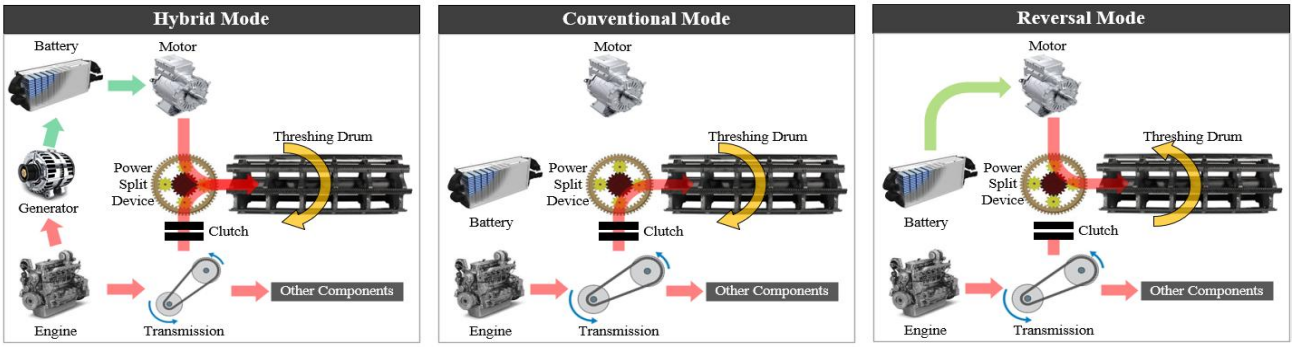

Fig. 2 - Three power mode of the DPSTD

DPSTD model

Dynamic model of the threshing drum

The active torque required by the threshing drum mainly includes the torque required for the idling of the drum itself, the torque to push the grain to overcome the resistance movement, the torque to overcome the angular acceleration generated by the rotational inertia of the drum itself, and the torque to push the grain to obtain acceleration. The total driving torque of threshing drum is

$$T_{TD} = A + B\omega_{TD}^{\ 2} + \frac{qR_{TD}^{\ 2}\omega_{TD}}{2(1-f_r)}\frac{\lambda+\Delta}{1+\Delta} + J_{TD}\dot{\omega}_{TD}$$

$$q = \rho v H \tag{1}$$

where ω_{TD} is the angular velocity of the drum, A is the torque to overcome mechanical friction, B is the air friction coefficient, q is the harvest quantity, ρ is the crop density, v is the travelling speed of the harvester, H is the cutting range, R_{TD} is the operating radius of threshing drum, Δ is the grass-grain ratio, f_r is the friction coefficient, J_{TD} is the rotational inertia of the threshing drum.

Model of the power coupling device

According to Fig.1, the power coupling device in the DPSTD consists of a reducer and a single-row planetary gear mechanism. The corresponding components are connected to the power output shaft of the engine, the motor, and the threshing drum, respectively, which closely relate the system's power transmission to the speed-torque characteristics of the power coupling device.

The output speed of the power coupling device can be expressed as:

$$\omega_{out} = \frac{(1+k)\omega_e - \omega_m / i_r}{k} \tag{2}$$

The output torque of the power coupling device can be expressed as:

$$T_{out} = -(\frac{T_m}{i_r \eta_r} + T_e) \tag{3}$$

where ω_e and ω_m are the speed of engine power output shaft and motor, T_e and T_m are the torque of engine power output shaft and motor, i_r is the gear ratio of the reducer, η_r is the efficiency of the reducer, and k is the ratio of the number of teeth on the outer planetary gear to the number of teeth on the sun gear.

It can be seen that the speed and torque of the threshing drum can be adjusted by adjusting the output speed and torque of the motor.

Torque coordination control of the DPSTD

As described previously regarding the DPSTD's three modes, its hybrid mode offers speed control and stability—features not found in conventional threshing drums—effectively enhancing the combine harvester's performance and versatility. Therefore, the torque coordination control of the DPSTD motor in hybrid mode is a key issue addressed in this study. During the operation of the harvester, complex and varying terrains, as well as uncertainties in crop attributes, will generate random and time-varying disturbances. These disturbances are transmitted through the powertrain, resulting in torque impacts and interferences on the threshing drum, which in turn affect the operational performance. Therefore, it is crucial to pay special attention to disturbance estimation and compensation under such conditions during the operation of DPSTD. Designing reliable control strategies is necessary to mitigate the performance fluctuations caused by torque disturbances. The key issues of torque coordination control in DPSTD operation in hybrid mode can be summarized in the following two aspects:

(1) A high-performance controller needs to be designed to accurately regulate the motor speed during the drum speed adjustment process, ensuring that the threshing drum operates at the desired speed and improving operational performance.

(2) To address unpredictable disturbances caused by varying terrains and crop attributes, it is necessary to design corresponding disturbance observers to estimate the disturbances and uncertainties, and then perform compensation control.

Based on the analysis of the hybrid mode of DPSTD mentioned above, a torque coordination control strategy for dual power sources is proposed. The strategy structure is illustrated in Fig. 3.

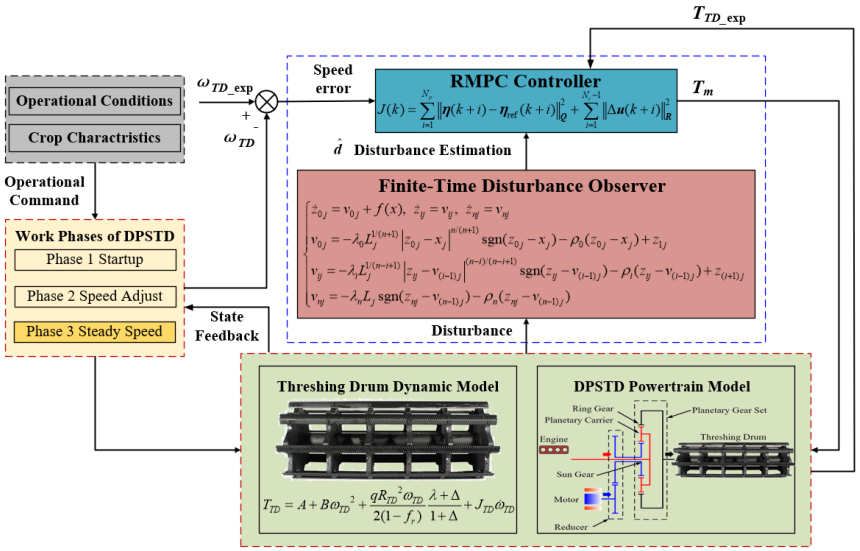

Fig. 3 - Control strategy structure of DPSTD

During the harvesting operation, the operator first sends instructions to the system according to the operating conditions and crop properties to determine the working stage and expected rotation speed of the threshing drum. The expected rotation speed of the threshing drum can be expressed as *(Li et al., 2009):*

$$\omega_{TD\_\exp} = \frac{60\sqrt{\frac{2R_{\max}}{m}}}{\pi D(1+\varepsilon)\cos\beta} \tag{4}$$

where $R_{\max}$ is the maximum work required to detach the grains from the spike, m is the mass of the grain, β is the angle between the axial direction of the grain and the direction of the axial movement of the threshing teeth, ε is the restitution coefficient during the impact between the grain and the threshing teeth, and D is the diameter of the threshing drum.

During harvesting operations, the engine power is generally kept relatively constant. Therefore, at the desired speed of the threshing drum, the target output speed of the motor is:

$$\omega_{m\_\text{tgt}} = i_r[(1+k)\omega_e - k\omega_{TD\_\exp}] \tag{5}$$

The preliminary target output torque of motor without considering disturbances is:

$$T_{m\_\text{tgt}} = -(T_e + T_{TD\_\exp})i_r\eta_r \tag{6}$$

where $T_{TD\_\exp}$ is the theoretical torque required by the threshing drum at the desired speed.

Based on this, in order to further achieve precise torque coordination control of the motor, a Robust Model Predictive Control (RMPC) controller is designed to regulate the motor torque. Furthermore, a Finite-Time Disturbance Observer (FTDO) is introduced to estimate the torque disturbances that exist during the harvesting process.

Design of the RMPC controller

Defining the speed of threshing drum and the speed of engine power output shaft as the state variables, motor output torque as the control variables, and the load fluctuation of threshing drum and the resistance torque of engine source as the disturbance variables, the dynamics equation of the threshing system can be written as the following state space equation:

$$\begin{cases} \dot{\boldsymbol{x}} = \boldsymbol{A}\boldsymbol{x} + \boldsymbol{B}\boldsymbol{u} + \boldsymbol{C} + \boldsymbol{\Gamma}\boldsymbol{d} \\ \boldsymbol{y} = \boldsymbol{D}\boldsymbol{x} \end{cases} \tag{7}$$

where the state variables $\boldsymbol{x} = \left[\omega_{TD}, \omega_{TD}^{\ 2}, \omega_e\right]^T$, $\boldsymbol{u}$ is the control variables, the disturbance variables $\boldsymbol{d} = \left[d_1, d_2\right]^T$,

$$\boldsymbol{A} = \begin{bmatrix} -\frac{qR_{TD}^{\ 2}}{2J_{TD}(1-f_r)} & \frac{\lambda+\Delta}{1+\Delta} & -\frac{B}{J_{TD}} & 0 \\ 2 & & 0 & 0 \\ 0 & & 0 & -\frac{c_e}{J_e} \end{bmatrix}, \boldsymbol{B} = \left[\frac{1}{J_{TD}i_r\eta_r}, 0, 0\right]^T, \boldsymbol{C} = \left[\frac{T_{TD}-A}{J_{TD}}, 0, \frac{T_e}{J_e}\right]^T, \boldsymbol{\Gamma} = \begin{bmatrix} \frac{1}{J_{TD}} & 0 \\ 0 & \frac{1}{J_e} \end{bmatrix}, \boldsymbol{D} = \left[1, 0, 0\right]^T,$$

c_e is the damping of the engine power output shaft, J_e is the rotational inertia of the engine power output shaft.

The forward Euler method is used to discretize the above state space equation, and the corresponding discretization form can be expressed as:

$$\begin{cases} \boldsymbol{x}(k+1) = \boldsymbol{A}_k\boldsymbol{x}(k) + \boldsymbol{B}_k\boldsymbol{u}(k) + \boldsymbol{C} + \boldsymbol{\Gamma}_k\boldsymbol{d}(k) \\ \boldsymbol{y}(k+1) = \boldsymbol{D}\boldsymbol{x}(k) \end{cases} \tag{8}$$

where $\boldsymbol{A}_k(T_s) = \boldsymbol{I} + T_s\boldsymbol{A}$, $\boldsymbol{B}_k(T_s) = T_s\boldsymbol{B}$, $\boldsymbol{\Gamma}_k(T_s) = T_s\boldsymbol{\Gamma}$.

A new model prediction equation is established according to the above formula, which is expressed as:

$$\xi(k) = \left[\boldsymbol{x}(k),\ \boldsymbol{u}(k-1)\right]^T \tag{9}$$

Then the system state space equation in incremental form can be written as:

$$\begin{cases} \xi(k+1) = \tilde{\boldsymbol{A}}_k\xi(k) + \tilde{\boldsymbol{B}}_k\boldsymbol{u}(k) + \tilde{\boldsymbol{\Gamma}}_k\boldsymbol{d}(k) + \boldsymbol{C} \\ \boldsymbol{\eta}(k) = \tilde{\boldsymbol{D}}\xi(k) \end{cases} \tag{10}$$

where $\tilde{\boldsymbol{A}}_k = \begin{bmatrix} \boldsymbol{A}_k & \boldsymbol{B}_k \\ 0_{m\times n} & \boldsymbol{I}_{m\times n} \end{bmatrix}$, $\tilde{\boldsymbol{B}}_k = \begin{bmatrix} \boldsymbol{B}_k \\ \boldsymbol{I}_{m\times n} \end{bmatrix}$, $\tilde{\boldsymbol{\Gamma}}_k = \begin{bmatrix} \boldsymbol{\Gamma}_k \\ \boldsymbol{I}_{m\times m} \end{bmatrix}$, $\tilde{\boldsymbol{D}} = [\boldsymbol{D} \quad 0 \quad 0]$, $\boldsymbol{\eta}(k)$ is the output variable, m is the dimension of the control variable, and n is the dimension of the state variable.

If the current time of the system is k, the prediction time domain is N_p, and the control time domain is N_c, and $N_c \le N_p$, then the system output vector at N_p step and the control increment vector at N_c step can be expressed as:

$$\begin{aligned} \boldsymbol{Y}(k) &= [\boldsymbol{\eta}(k+1\,|\,k), \boldsymbol{\eta}(k+2\,|\,k), \cdots, \boldsymbol{\eta}(k+N_p\,|\,k)] \\ \Delta\boldsymbol{u}(k) &= [\Delta\boldsymbol{u}(k), \Delta\boldsymbol{u}(k+1), \cdots, \Delta\boldsymbol{u}(k+N_c)-1] \end{aligned} \tag{11}$$

The output of the system at step N_p can be calculated by the prediction equation in the following form:

$$\boldsymbol{Y}(k) = \boldsymbol{S}_{\xi}\boldsymbol{\xi}(k) + \boldsymbol{S}_u\Delta\boldsymbol{u}(k) + \boldsymbol{S}_{\omega}\Delta\boldsymbol{d}(k) \tag{12}$$

where $\boldsymbol{S}_{\xi} = \begin{bmatrix} \tilde{C}_{dk}\tilde{A}_{dk} \\ \tilde{C}_{dk}\tilde{A}_{dk}^2 \\ \vdots \\ \tilde{C}_{dk}\tilde{A}_{dk}^{N_c} \\ \vdots \\ \tilde{C}_{dk}\tilde{A}_{dk}^{N_p} \end{bmatrix}$, $\boldsymbol{S}_{\omega} = \begin{bmatrix} \tilde{C}_{dk}\tilde{\Gamma}_{dk} \\ \tilde{C}_{dk}\tilde{\Gamma}_{dk}^2 \\ \vdots \\ \tilde{C}_{dk}\tilde{\Gamma}_{dk}^{N_c} \\ \vdots \\ \tilde{C}_{dk}\tilde{\Gamma}_{dk}^{N_p} \end{bmatrix}$, $\boldsymbol{S}_u = \begin{bmatrix} \tilde{C}_{dk}\tilde{B}_{dk} & 0 & 0 & \cdots & 0 \\ \tilde{C}_{dk}\tilde{A}_{dk}\tilde{B}_{dk} & \tilde{C}_{dk}\tilde{B}_{dk} & 0 & \cdots & 0 \\ \cdots & \cdots & \vdots & \ddots & \vdots \\ \tilde{C}_{dk}\tilde{A}_{dk}^{N_c-1}\tilde{B}_{dk} & \tilde{C}_{dk}\tilde{A}_{dk}^{N_c-2}\tilde{B}_{dk} & \cdots & \cdots & \tilde{C}_{dk}\tilde{B}_{dk} \\ \tilde{C}_{dk}\tilde{A}_{dk}^{N_c}\tilde{B}_{dk} & \tilde{C}_{dk}\tilde{A}_{dk}^{N_c-1}\tilde{B}_{dk} & \cdots & \cdots & \tilde{C}_{dk}\tilde{A}_{dk}\tilde{B}_{dk} \\ \vdots & \vdots & \vdots & \ddots & \vdots \\ \tilde{C}_{dk}\tilde{A}_{dk}^{N_p-1}\tilde{B}_{dk} & \tilde{C}_{dk}\tilde{A}_{dk}^{N_p-2}\tilde{B}_{dk} & \cdots & \cdots & \tilde{C}_{dk}\tilde{A}_{dk}^{N_p-N_c-1}\tilde{B}_{dk} \end{bmatrix}$

According to the prediction equation, the reference vector of the system can be expressed as:

$$\boldsymbol{\eta}_{\text{ref}}(k) = [\boldsymbol{\eta}_{\text{ref}}(k+1\,|\,k), \boldsymbol{\eta}_{\text{ref}}(k+2\,|\,k), \cdots, \boldsymbol{\eta}_{\text{ref}}(k+N_p\,|\,k)] \tag{13}$$

Therefore, the system objective function with quadratic form corresponding to the RMPC controller can be expressed as:

$$J(k) = \sum_{i=1}^{N_p} \|\boldsymbol{\eta}(k+i) - \boldsymbol{\eta}_{\text{ref}}(k+i)\|_{\boldsymbol{Q}}^2 + \sum_{i=1}^{N_c-1} \|\Delta\boldsymbol{u}(k+i)\|_{\boldsymbol{R}}^2 \tag{14}$$

where $\boldsymbol{\eta}_{\text{ref}}$ is the reference vector of system, $\boldsymbol{Q}$ and $\boldsymbol{R}$ are the weight coefficient matrix of output and control of system respectively.

The objective function reflects the tracking error and control quantity. It can be transformed into a standard quadratic form, which is easy to solve, so as to minimize the tracking error and control increment.

According to the output of system, the reference vector of system can be written as:

$$\boldsymbol{\eta}_{\text{ref}} = [\omega_{TD\_\text{ref}}] \tag{15}$$

The weight coefficient matrix of output and control quantity of system is:

$$\begin{cases} \boldsymbol{Q} = diag([w_{\omega_{TD}}]) \\ \boldsymbol{R} = diag([w_{T_m}]) \end{cases} \tag{16}$$

The deviation within the prediction range is defined as:

$$\boldsymbol{E}(k) = \boldsymbol{S}_{\xi}\boldsymbol{\xi}(k) - \boldsymbol{\eta}_{\text{ref}}(k+1) \tag{17}$$

The objective function of the system can be transformed into a standard quadratic form and expressed as:

$$J(\Delta\boldsymbol{U}(k)) = \begin{bmatrix} \Delta\boldsymbol{U}(k) \\ \varepsilon \end{bmatrix}^{\mathrm{T}} \boldsymbol{H} \begin{bmatrix} \Delta\boldsymbol{U}(k) \\ \varepsilon \end{bmatrix} + \boldsymbol{G} \begin{bmatrix} \Delta\boldsymbol{U}(k) \\ \varepsilon \end{bmatrix} \tag{18}$$

where $\boldsymbol{H} = \begin{bmatrix} \boldsymbol{S}_u^{\mathrm{T}}\boldsymbol{Q}'\boldsymbol{S}_u + \boldsymbol{R} & 0 \\ 0 & \rho \end{bmatrix}$, $\boldsymbol{G} = [2\boldsymbol{E}(k)^{\mathrm{T}}\boldsymbol{Q}'\boldsymbol{S}_u \quad 0]$.

The constraints of system state, control quantity and output variable are respectively defined as:

$$\begin{cases} \Delta\boldsymbol{U}_{\min} \le \Delta\boldsymbol{U} \le \Delta\boldsymbol{U}_{\max} \\ \boldsymbol{U}_{\min} \le A\Delta\boldsymbol{U} + \boldsymbol{U} \le \boldsymbol{U}_{\max} \\ \boldsymbol{Y}_{\min} - \varepsilon \le \boldsymbol{S}_{\xi}\boldsymbol{\xi}(k) + \boldsymbol{S}_u\Delta\boldsymbol{U}(k) \le \boldsymbol{Y}_{\max} + \varepsilon \end{cases} \tag{19}$$

where $\Delta\boldsymbol{U}$ is the increment of control quantity.

By solving the quadratic programming problem in each control domain, a series of increments of control input in the control domain can be calculated:

$$\Delta \boldsymbol{U}^* = \left[\Delta \boldsymbol{u}^*(k), \Delta \boldsymbol{u}^*(k+1), \Delta \boldsymbol{u}^*(k+2), \cdots, \Delta \boldsymbol{u}^*(k+N_c-1)\right]^{\mathrm{T}} \tag{20}$$

Therefore, the control input of motor torque can be calculated by the following formula:

$$\boldsymbol{u}(k) = \boldsymbol{u}(k-1) + \Delta \boldsymbol{U}^* \tag{21}$$

Design of the FTDO

The FTDO is further introduced to estimate the disturbance variables. For the system with the form of Eq. (7), the system disturbance satisfies the following conditions: the disturbance term d_i is *n*-order continuously differentiable (where *n* represents the system order), and its *j*-order derivative is bounded and satisfies $\left|d_i^{(j)}\right| \le L_i$, where $L_i > 0$, $i = 1, \cdots, n$, and $j = 0, 1, \cdots, n$.

The FTDO to be designed has the following standard forms:

$$\begin{cases} \dot{z}_{0j} = v_{0j} + f(x) \\ \dot{z}_{ij} = v_{ij} \\ \dot{z}_{nj} = v_{nj} \\ v_{0j} = -\lambda_0 L_j^{1/(n+1)} \left|z_{0j} - x_j\right|^{n/(n+1)} \operatorname{sgn}(z_{0j} - x_j) - \rho_0 (z_{0j} - x_j) + z_{1j} \\ v_{ij} = -\lambda_i L_j^{1/(n-i+1)} \left|z_{ij} - v_{(i-1)j}\right|^{(n-i)/(n-i+1)} \operatorname{sgn}(z_{ij} - v_{(i-1)j}) - \rho_i (z_{ij} - v_{(i-1)j}) + z_{(i+1)j} \\ v_{nj} = -\lambda_n L_j \operatorname{sgn}(z_{nj} - v_{(n-1)j}) - \rho_n (z_{nj} - v_{(n-1)j}) \end{cases} \tag{22}$$

where $\lambda_0, \cdots, \lambda_n$ and $\rho_0, \cdots, \rho_n$ are the pending coefficients of the FTDO respectively. z_{0j} is the estimated value of the state variable. $z_{1j}, \cdots, z_{nj}$ are the estimated values of the disturbance quantity $d_j^{(0)}, \cdots, d_j^{(n-1)}$ respectively. $i = 1, \cdots, n-1$, $j = 1, \cdots, n$, and $f(x)$ corresponds to the equation of state shown in Eq. (7).

When $j = 1$ and $j = 2$ respectively, the torque disturbance can be estimated by the following FTDO equation respectively:

$$\begin{cases} \dot{z}_{01} = v_{01} + f(x_1) \\ \dot{z}_{11} = v_{11} \\ \dot{z}_{21} = v_{21} \\ v_{01} = -\lambda_0 L_1^{1/3} \left|z_{01} - x_1\right|^{2/3} \operatorname{sgn}(z_{01} - x_1) - \rho_0 (z_{01} - x_1) + z_{11} \\ v_{11} = -\lambda_1 L_1^{1/2} \left|z_{11} - v_{01}\right|^{1/2} \operatorname{sgn}(z_{11} - v_{01}) - \rho_1 (z_{11} - v_{01}) + z_{21} \\ v_{21} = -\lambda_2 L_1 \operatorname{sgn}(z_{21} - v_{11}) - \rho_2 (z_{21} - v_{11}) \end{cases} \quad \begin{cases} \dot{z}_{02} = v_{02} + f(x_3) \\ \dot{z}_{12} = v_{12} \\ \dot{z}_{22} = v_{22} \\ v_{02} = -\lambda_0 L_2^{1/3} \left|z_{02} - x_2\right|^{2/3} \operatorname{sgn}(z_{02} - x_2) - \rho_0 (z_{02} - x_2) + z_{12} \\ v_{12} = -\lambda_1 L_2^{1/2} \left|z_{12} - v_{02}\right|^{1/2} \operatorname{sgn}(z_{12} - v_{02}) - \rho_1 (z_{12} - v_{02}) + z_{22} \\ v_{22} = -\lambda_2 L_2 \operatorname{sgn}(z_{22} - v_{12}) - \rho_2 (z_{22} - v_{12}) \end{cases} \tag{23}$$

where: z_{01} and z_{02} are the estimated values of the state quantity ω_{TD} and ω_e respectively. z_{11} and z_{12} are the estimated values of disturbance d_1 and d_2 respectively. z_{21} and z_{22} are the estimated values of $\dot{d}_1$ and $\dot{d}_2$ respectively.

To further analyze the stability and convergence of the proposed FTDO, the above estimation errors are defined as:

$$\sigma_{0j} = \frac{z_{0j} - x_j}{L_j}, \sigma_{1j} = \frac{z_{1j} - d_j}{L_j}, \cdots, \sigma_{nj} = \frac{z_{nj} - d_j^{(n-1)}}{L_j} \tag{24}$$

From Eq. (9), the differential form of Eq. (24) can be obtained as follows:

$$\dot{\sigma}_{0j} = -\lambda_0 \left|L_j \sigma_{0j}\right|^{n/(n+1)} \operatorname{sgn}(\sigma_{0j}) - \rho_0 \sigma_{0j} + \sigma_{1j} \tag{25}$$

Similarly:

$$\dot{\sigma}_{1j} = \frac{1}{L_j}\left(-\lambda_1 L_j^{1/(n+1)} \left|z_{1j} - v_{0j}\right|^{(n-1)/n} \operatorname{sgn}(z_{1j} - v_{0j}) - \rho_1 (z_{1j} - v_{0j})\right) + \sigma_{2j} \tag{26}$$

It can be seen that:

$$z_{1j} - v_{0j} = \lambda_0 L_j \left|\sigma_{0j}\right|^{n/(n+1)} \operatorname{sgn}(\sigma_{0j}) + \rho_0 (L_j \sigma_{0j}) = L_j (\sigma_{1j} - \dot{\sigma}_{0j}) \tag{27}$$

Then, substituting Eq. (27) into Eq. (26) yields:

$$\dot{\sigma}_{1j} = -\lambda_1 \left|\sigma_{1j} - \dot{\sigma}_{0j}\right|^{(n-1)/n} \operatorname{sgn}(\sigma_{1j} - \dot{\sigma}_{0j}) - \rho_1 (\sigma_{1j} - \dot{\sigma}_{0j}) + \sigma_{2j} \tag{28}$$

Similarly, for i = 2, …, n-1, it follows that:

$$\dot{\sigma}_{ij} = -\lambda_i \left|\sigma_{ij} - \dot{\sigma}_{(i-1)j}\right|^{(n-i)/(n-i+1)} \operatorname{sgn}(\sigma_{ij} - \dot{\sigma}_{(i-1)j}) - \rho_i (\sigma_{ij} - \dot{\sigma}_{(i-1)j}) + \sigma_{(i+1)j} \tag{29}$$

$$\dot{\sigma}_{nj} = -\lambda_n \operatorname{sgn}(\sigma_{nj} - \dot{\sigma}_{(n-1)j}) - \rho_n (\sigma_{nj} - \dot{\sigma}_{(n-1)j}) + \frac{1}{L_j} d_j^n \tag{30}$$

Therefore, the estimation error of the FTDO can be expressed as follows:

$$\begin{aligned}
&\dot{\sigma}_{0j} = -\lambda_0 \left|\sigma_{0j}\right|^{n/(n+1)} \operatorname{sgn}(\sigma_{0j}) - \rho_0 (\sigma_{0j}) + \sigma_{1j} \\
&\vdots \\
&\dot{\sigma}_{(n-1)j} = -\lambda_{n-1} \left|\sigma_{(n-1)j} - \dot{\sigma}_{(n-2)j}\right|^{1/2} \operatorname{sgn}(\sigma_{(n-1)j} - \dot{\sigma}_{(n-2)j}) - \rho_{n-1} (\sigma_{(n-1)j} - \dot{\sigma}_{(n-2)j}) + \sigma_{nj} \\
&\dot{\sigma}_{nj} = -\lambda_n \operatorname{sgn}(\sigma_{nj} - \dot{\sigma}_{(n-1)j}) - \rho_n (\sigma_{nj} - \dot{\sigma}_{(n-1)j}) + \frac{1}{L_j} d_j^n
\end{aligned} \tag{31}$$

According to the relevant research conclusions *(Nguyen et al, 2021)*, it can be seen that the system (31) is stable in finite time, indicating that the estimation error of the FTDO can converge to zero in finite time.

Then the compensation torque of motor is:

$$\boldsymbol{u} = T_{m\_\mathrm{com}} = -i_r \eta_r (z_{21} + z_{22}) \tag{32}$$

RESULTS AND DISCUSSION

The previous section focused on the control methods of the designed DPSTD in hybrid mode, specifically addressing the regulation of drum speed for combined harvester operation, as well as its resistance to disturbance and overload. To explore the effectiveness of the DPSTD's structure and control methods proposed in this paper, a simulation model of the DPSTD was further developed using the MATLAB/Simulink platform. The simulation includes the performance evaluation of the designed FTDO, speed control functions of the DPSTD, as well as a comparison of the proposed control method's effectiveness in suppressing disturbances and load fluctuations with and without disturbance compensation.

Verification of the FTDO performance

Assuming that the combine harvester experiences a random disturbance torque from the engine power source during the harvesting process, characterized by Gaussian white noise with a sampling time of 0.01, a variance of 30, and a mean of 0. This disturbance torque is applied to the actual output torque of the DPSTD engine power input shaft. The results of the state estimation and the disturbance estimation of the FTDO during the operation of the DPSTD are shown in Fig. 4.

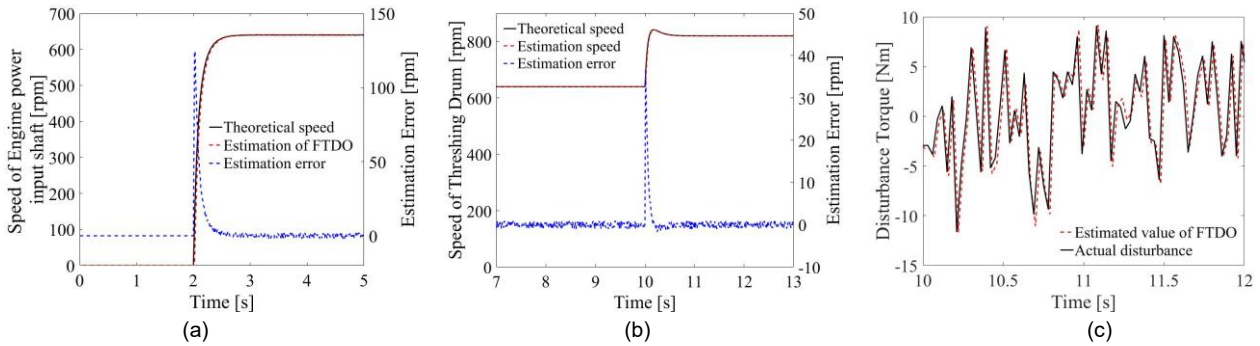

Fig. 4 -The result of the FDTO estimation

(a) State estimation (speed of engine power input shaft); (b) State estimation (speed of threshing drum); (c) disturbance estimation

Fig. 4(a) and Fig. 4(b) show the variations of the two state variables of the speed of engine power input shaft and threshing drum obtained by the FTDO during the estimation of random disturbance. The engine startup process begins at approximately 2.0 s, while the speed adjustment process of the threshing drum starts at 10.0 s. It can be observed that the FTDO accurately estimates the speed of engine power input shaft and the threshing drum with small estimation errors and convergence stability within a finite time. Fig. 4(c) represents the estimated disturbance torque obtained by the FTDO, which exhibits the same trend with the actual values and demonstrates good estimation accuracy.

Simulation of torque dynamic compensation control of the DPSTD

A control simulation analysis of the DPSTD torque compensation control was performed to test its anti-interference and overload resistance capabilities. Assume that the target speed of the DPSTD is from 660 rpm to 770 rpm, and there is a random disturbance torque during the operation. Additionally, a step change in load of 20 Nm occurs at the 8th second. Fig. 5 compares the effects of the DPSTD with torque compensation control based on FTDO and without compensation control under the influence of torque disturbances and load transients.

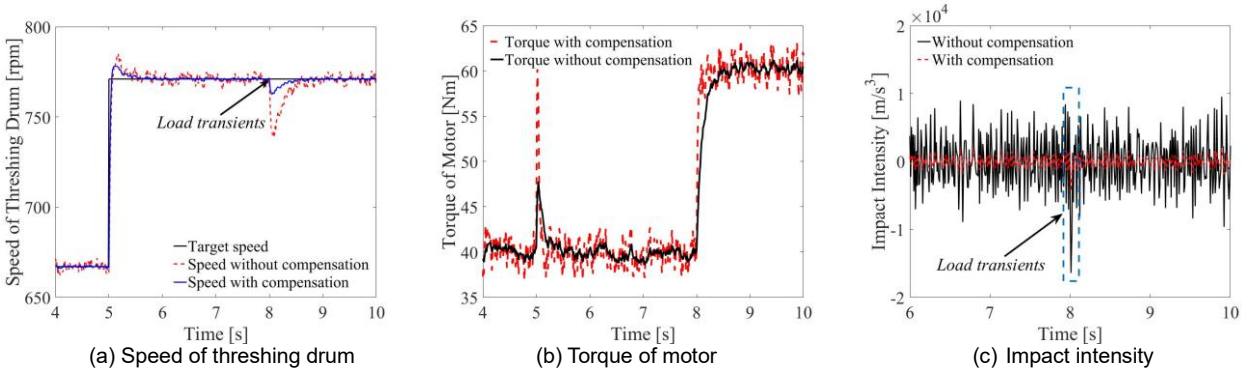

(a) Speed of threshing drum (b) Torque of motor (c) Impact intensity

Fig. 5 - Comparison of torque compensation control

From Fig. 5(a) and Fig. 5(b), it can be observed that when the DPSTD does not employ any interference compensation control strategy, the torque disturbances significantly deteriorate the smoothness of the threshing drum speed tracking. Additionally, these disturbances are not detected by the upper-level controller, and the torque command to the motor continues to be issued by the basic torque controller. However, when employing the FTDO interference compensation control strategy, the current disturbance signal value can be estimated, and subsequently, the output torque of the motor is recalculated, which greatly reduces the impact of the DPSTD, improves the stability of speed tracking, and enhances the quality of mode switching.

Furthermore, according to the simulation results of load transients starting at the 8th seconds in Fig. 5(c), when there is no torque compensation control, the output load transients greatly deteriorate the operation quality of the DPSTD, causing an impact with an amplitude of $1.64 \cdot 10^4$ m/s^3, and the speed tracking shows obvious oscillation. However, the torque compensation control based on FTDO accurately estimates the load changes and coordinates the output torque of the motor, effectively limiting the impact within the range of [$-0.45 \cdot 10^4$ m/s^3, $0.45 \cdot 10^4$ m/s^3]. It also reduces the speed oscillations, achieving a smoother speed tracking. Table 1 presents a comparison of the effects with and without torque compensation control. It can be observed that the control strategy with compensation significantly reduces the impact and speed errors of DPSTD. The root mean square (RMS) value of speed errors is decreased by 73.90%, the maximum speed error id decreased by 76.18%, the RMS value of impact is decreased by 33.51%, and the maximum impact is reduced by 73.18%. In conclusion, the designed torque compensation control strategy based on FTDO can significantly improve the smoothness of mode switching and the speed tracking of the threshing drum, making the DPSTD has a strong anti-interference capability.

Table 1

Comparison of control effects based on two strategies

Control strategy	RMS of speed error (rpm)	Maximum speed error (rpm)	RMS of impact intensity (m/s^3)	Maximum impact intensity (m/s^3)
Without compensation	32.64	31.32	1.94×10^3	1.64×10^4
With compensation	8.52	7.46	1.29×10^3	0.43×10^4

Bench test

In order to verify the feasibility of the structure and control strategy of the DPSTD, a bench test is carried out based on a testing platform. It should be noted that due to the limitations of the experimental equipment, the engine test cannot be realized but considering that the purpose of the test is to verify the effectiveness of the control strategy in the presence of torque disturbances from the engine source, the motor can be used to simulate this part of the torque disturbance. Fig. 6 is the schematic diagram of testing platform for the DPSTD, which is mainly composed of a multi-functional power coupling device (with two built-in motors), two electric dynamometers (corresponding to the left and right driving semi-axis respectively), a testing platform controller and related auxiliary equipment. The functionality of reading the status parameters of the power coupling device, load simulation of the electric dynamometers, and parameter settings and status monitoring of the upper computer can be achieved through CAN bus communication. The multi-functional power coupling device can be used to simulate the power coupling device in the DPSTD, while one of its built-in motors emulating the engine source power, while the other one acts as the driving motor in the DPSTD. Additionally, the electric dynamometers are used to simulate the load input.

Fig. 6 - The testing platform

The designed observer and controller are integrated into the motor controller application layer of the testing platform, enabling the application of the designed control strategy. Fig.7 presents the bench test results of the DPSTD applying the torque compensation control strategy during mode switching, speed regulation, and when subjected to load transients.

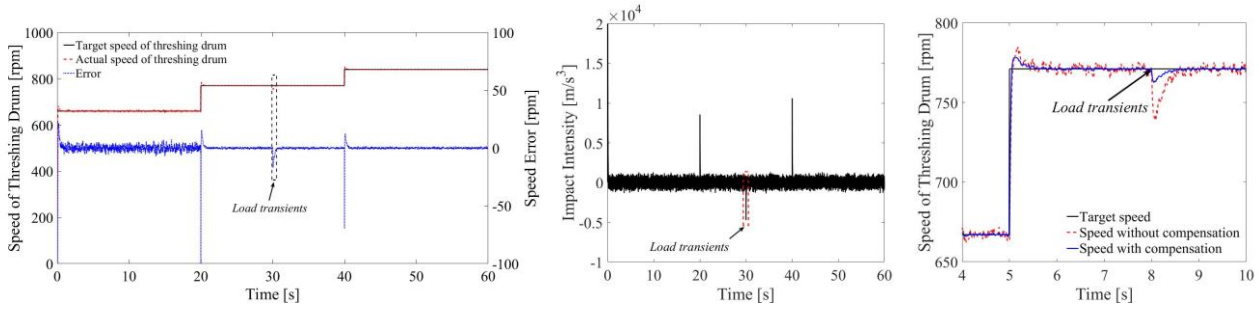

Fig. 7 - The results of bench test

(a) Speed of threshing drum; (b) Impact intensity; (c) Torque of motor and engine power input shaft

It can be observed from Fig. 7(a) that in the bench test, the actual speed of the threshing drum is closely aligned with the target speed, with only significant errors occurring during demand speed transients. This is attributed to the controller response and communication delays in the experiment. However, the error duration is short and will not significantly affect the performance. Hence, the errors generated in this case can be disregarded. Additionally, in the conventional mode where the motor is not engaged, the speed error is noticeably higher compared to the hybrid mode. This observation demonstrates that the DPSTD employing motor disturbance compensation control can effectively improve speed tracking accuracy. Fig. 7(b) shows that compared to the simulation results with compensation control, the bench test exhibits higher impact intensity but remains within 1.1×10^4 m/s^3. During load transients, the impact intensity is slightly higher than the simulation results, but the overall effect is still satisfactory.

It can be seen from Fig. 7(c) that the driving motor can promptly start and engage during mode switching, accomplishing the speed regulation function of the DPSTD. Simultaneously, effective torque compensation can be achieved to mitigate disturbances and load transients, reducing speed oscillations and minimizing torque shocks in the transmission system.

To sum up, compared with the closed simulation environment, the bench test results are different from the simulation results due to the differences in equipment parameters, motor performance, communication and control time delay and other factors, but still achieved satisfactory outcomes. The test verifies that the designed DPSTD possesses sensitive and versatile speed regulation capabilities, enhancing the versatility of the combine harvester. Additionally, the proposed motor control method realizes disturbance identification and compensation control, improving the DPSTD's anti-interference ability during operation, thereby ensuring stable operational performance. Consequently, the superiority of the DPSTD's threshing system over that of conventional combine harvesters is demonstrated.

CONCLUSIONS

Based on a parallel hybrid system, this study proposes a dual power source threshing drum that can be driven by both an engine and an electric motor. A RMPC controller is designed for the motor control, and FTDO are incorporated to enhance the control performance. The study further explores the performance of the DPSTD, including its speed regulation capability and disturbance rejection ability. Finally, a bench test is conducted to validate the effectiveness and superiority of the DPSTD. According to the findings above, the following conclusions were reached:

(1) Compared to conventional threshing drums, the DPSTD driven by engine and motor can use the large-scale speed regulation function of motor to realize the adjustable speed of threshing drum in hybrid mode, and has fast dynamic response, allowing for quick parameter adjustments according to the harvesting requirements of different crops, enabling versatile applications.

(2) The RMPC controller for motor based on the FTDO can accurately estimate the disturbance torque and operating load during operation, enabling fast and precise torque compensation. Simulation results show that, in the presence of torque disturbances and load transients, the control strategy with torque compensation reduces the RMPC value of speed error by 73.90%, the maximum speed error by 76.18%, the RMPC value of impact intensity by 33.51%, and the maximum impact intensity by 73.18% compared to the control strategy without compensation. This approach significantly improves smoothness of mode switching and speed tracking performance of the threshing drum, demonstrating excellent anti-interference ability.

(3) The bench test demonstrates that the designed DPSTD with torque compensation can effectively perform speed adjustment and exhibits anti-interference ability. The test results are similar to the simulation results, which proves the rationality and effectiveness of the designed DPSTD in terms of its structure and control strategy, and provides a novel and valuable reference for the research on the speed control of threshing drum of combine harvester.

ACKNOWLEDGMENTS

The authors gratefully acknowledge the Jiangsu Agricultural Science and Technology Innovation Fund (CX[22]1005), the Project of Faculty of Agricultural Equipment of Jiangsu University (NZXB20210103), the Postgraduate Research & Practice Innovation Program of Jiangsu Province (KYCX23_3668), the Major Scientific and Technological Special Project of Anhui Province (202203a06020025) and the National Natural Science Foundation of China (52405271) for the financial support.

REFERENCES

[1] Alizadeh, M. R., Khodabakhshipour, M. (2010). Effect of threshing drum speed and crop moisture content on the paddy grain damage in axial-flow thresher. *Agronomical Research in Moldavia (Cercetări Agronomice în Moldova)*, *4*(144), 5-11. https://repository.iuls.ro/xmlui/handle/20.500.12811/2571

[2] Chen, J., Ning, X., Li, Y., Yang, G., Wu, P., Chen, S. (2017). A fuzzy control strategy for the forward speed of a combine harvester based on KDD. *Applied engineering in agriculture*, *33*(1), 15-22. https://doi.org/10.13031/aea.11299

[3] Hou, Y., Shang, S., Li, X., He, X.N., Zheng, H., Dong, T., Li, X., Liu, Z., Yang, S., Wang, D.W. (2023). Discrete element method (EDEM) simulation and parameter optimization design and testing of a low-loss and high-efficiency corn threshing device. *INMATEH – Agricultural Engineering 71*(3), 194-204. https://doi.org/10.35633/inmateh-71-16

[4] Khatawkar, D.S. James, P. S., Dhalin, D. (2019). Modern trends in farm machinery-electric drives: A Review. *International Journal of Current Microbiology and Applied Sciences*, (8), 83-98. https://doi.org/10.20546/ijcmas.2019.801.011.

[5] Li, B. (2009). *Agricultural Mechanics (农业机械)*. Beijing, China Agriculture Press. (in Chinese)

[6] Li, H., Wang, Q., Wang, Y., Ma, J., Yue, D., Geng, D. (2023). Design and experiment of transverse axial flow corn flexible threshing device. *INMATEH – Agricultural Engineering, 69*(1), 461-470. https://doi.org/10.35633/inmateh-69-43

[7] Mocera, F., Somà, A. (2022). A Review of Hybrid Electric Architectures in Construction, Handling and Agriculture Machines. *New Perspectives on Electric Vehicles*, *49.* https://doi.org/10.5772/intechopen.99132

[8] Nguyen, N. P., Oh, H., Kim, Y., Moon, J., Yang, J., Chen, W. H. (2021). Finite-time disturbance observer-based modified super-twisting algorithm for systems with mismatched disturbances: Application to fixed-wing UAVs under wind disturbances. *International Journal of Robust and Nonlinear Control*, *31*(15), 7317-7343. https://doi.org/10.1002/rnc.5678

[9] Olaye, A. R. I. B., Moreira, J., Hounhouigan, J., Amponsah, S. K., Hounhouigan, D. J. (2016). Effect of threshing drum speed and crop weight on paddy grain quality in axial-flow thresher (ASI). *Journal of Multidisciplinary Engineering Science and Technology*, *3*(1), 3716-3721. https://www.researchgate.net/publication/305618996

[10] Qin, Y., Zhao, D., Li, Z., & Ji, W. (2009). Constant speed control of threshing drum of combine harvester based on RBF network (基于 RBF 网络的联合收获机脱粒滚筒恒速控制). *Transactions of the Chinese Society for Agricultural Machinery*, *40*(11), 59-63. *(in Chinese)*

[11] Sahoo, A. U., & Raheman, H. (2020). Development of an electric reaper: a clean harvesting machine for cereal crops. *Clean Technologies and Environmental Policy*, *22*, 955-964. https://doi.org/10.1007/s10098-020-01838-7

[12] Scolaro, E. Beligoj, M., & Estevez, M, P. (2021). Electrification of Agricultural Machinery: A Review. *IEEE Access*, (9), 164520-164541. https://doi.org/10.1109/ACCESS.2021.3135037.

[13] Shojaei, K. (2021). Intelligent coordinated control of an autonomous tractor-trailer and a combine harvester. *European Journal of Control*, *59*, 82-98. https://doi.org/10.1016/j.ejcon.2021.02.005.

[14] Sudajan, S., Salokhe, V. M., & Triratanasirichai, K. (2002). PM—Power and machinery: effect of type of drum, drum speed and feed rate on sunflower threshing. *Biosystems engineering*, *83*(4), 413-421. https://doi.org/10.1006/bioe.2002.0133.

[15] Sun, D. Chen, D., & Wang, S, M. (2018). Development on electrical system performance test stand for combine harvester. *Proceedings of the 6th International-Federation-of-Automatic-Control (IFAC) Conference on Bio-Robotics*, 2(7), 13-15. https://doi.org/10.1016/j.ifacol.2018.08.195.

[16] Vlădut, N.-V., Biris, S.St., Cârdei, P., Găgeanu, I., Cujbescu, D., Ungureanu, N., Popa, L.-D., Perişoară, L., Matei, G., Teliban, G.-C. (2022). Contributions to the Mathematical Modeling of the Threshing and Separation Process in an Axial Flow Combine. *Agriculture, 12*(10), 1520. https://doi.org/10.3390/agriculture12101520

[17] Vlădut, N.-V., Ungureanu, N., Biris, S.St., Voicea, I., Nenciu, F., Găgeanu, I., Cujbescu, D., Popa, L.-D., Boruz, S., Matei, G., Ekielski, A., Teliban, G.C. (2023). Research on the identification of some optimal threshing şi separation regimes in the axial flow apparatus. *Agriculture, 13*(4), 838. 10.3390/agriculture13040838, agriculture-2301663

[18] Wang, P., Tian, M., Wang, H., Jiang, W., Cao, Q. (2020). Electrical Modification and Experimental Study of Combine Harvester Reaping Unit. In *IOP Conference Series: Materials Science and Engineering*, *790*(1), 012168. https://doi.org/10.1088/1757-899X/790/1/012168.

[19] Yang, Z., Wang, H., Sun, H., Wang, P., Cao, Q. (2022). Experimental Study on Electric Harvesting of Combine Harvester. In *Journal of Physics: Conference Series*, *2218*(1), 012064. https://doi.org/10.1088/1742-6596/2218/1/012064.

[20] Zhang, J., Zhao, B., Yan, X., Liu, M., Xu, L., & Shang, C. (2023). Design and optimization of dual-motor electric tractor drive system based on driving cycles. *Plos one*, *18*(6), e0286378. https://doi.org/10.1371/journal.pone.0286378.

[21] Zhang, J., Zhao, D., Shen, H. (2011). Robust predictive control of threshing drum speed of combine harvester. *Control engineering of China*, *18*(4), 568-571.

[22] Zhang, Z., Jiang, H., He, X., Zhang, F., Wang, J., Wang, D. (2024). Design and test of threshing and cleaning device for Cyperus Esculentus L. combine harvester. *INMATEH – Agricultural Engineering* *72*(1), 798-808. https://doi.org/10.35633/inmateh-72-71

[23] Zhu, Z., Chai, X., Xu, L., Quan, L., Yuan, C., & Tian, S. (2023). Design and performance of a distributed electric drive system for a series hybrid electric combine harvester. *Biosystems Engineering*, *236*, 160-174. https://doi.org/10.1016/j.biosystemseng.2023.10.015.